INTERNATIONAL ATOMIC ENERGY AGENCY
UNITED NATIONS EDUCATIONAL, SCIENTIFIC AND CULTURAL ORGANIZATION
INTERNATIONAL CENTRE FOR THEORETICAL PHYSICS
I.C.T.P., P.O. BOX 586, 34100 TRIESTE, ITALY, CABLE: CENTRATOM TRIESTE

1

SMR.550 - 19

SPRING COLLEGE IN MATERIALS SCIENCE ON
"NUCLEATION, GROWTH AND SEGREGATION IN MATERIALS
SCIENCE AND ENGINEERING"
(6 May - 7 June 1991)

ELECTRON PROBE MICROANALYSIS AND RAMAN SPECTROSCOPY

P.R. GRAVES
AEA Industrial Technology
Harwell Laboratory
Didcot
Oxfordshire OX11 ORA
United Kingdom

These are preliminary lecture notes, intended only for distribution to participants.

Raman spectroscopy and electron probe microanalysis

Lecture 1: Raman spectroscopy- simplified theory, instrumentation, analytical applications to materials science

Lecture 2: Electron probe microanalysis- theory, instrumentation, application to high temperature corrosion. Raman spectroscopy phase determination in crystal growth of high temperature superconductors, characterisation of surface phases on high temperature superconductors.

Lecture 3: More advanced Raman spectroscopy- polarisation measurement, factor group analysis, lattice defect characterisation, thin film stress measurement.

SUPPLEMENT—Recent Scientific and Technical Books.

NOT TO BE REMOVED FROM

NATURE

A WEEKLY JOURNAL OF SCIENCE

"To the solid ground
Of Nature trusts the mind which builds for aye."—WORDSWORTH.

No. 3048, VOL. 121] SATURDAY, MARCH 31, 1928 [PRICE ONE SHILLING

[All Rights Reserved.

RESEARCH ESTAB LIBRARY MAY 1947 ARWELL

NEWTON'S "POPULAR" DEMONSTRATOR'S LANTERN

NEW MODEL (1928) PRICE £20

Open stage for the projection of slides or apparatus in vertical or horizontal position.

NEWTON & CO.

72 WIGMORE STREET, LONDON, W.1

REYNOLDS & BRANSON, Ltd.

"RYSTOS" MICROSCOPE LAMP

14 COMMERCIAL STREET, LEEDS.

BAIRD & TATLOCK (LONDON) LTD.

HOSSACK CLAMPS

(Patent No. 29526 27/11/23)

ADVANTAGES

Further particulars and prices on application.

SOLE ADDRESS:

14-15 CROSS STREET HATTON GARDEN LONDON E.C.1

NEGRETTI & ZAMBRA

38 HOLBORN VIADUCT LONDON, E.C.1.

RECORDING THERMOMETERS

RAMAN SPECTROSCOPY

KEY POINTS

- NON-DESTRUCTIVE
- NON-INVASIVE
- USES VISIBLE LIGHT
- GIVES CHEMICAL AND STRUCTURAL INFORMATION
- CAN BE USED IN ALMOST ANY ENVIRONMENT

3

[illegible] actors which determine the Occurrence of the Green Ray

[illegible] recent [illegible] ssion of the green ray which has [illegible] appearing in NATURE prompts me to put on [illegible] a new theory of the phenomenon which occurred [illegible] several years ago, but which I have refrained [illegible] publishing in the hope of securing proof. First [illegible] say most emphatically that the phenomenon [illegible] and not an illusion or after image. No person [illegible] in the observation of optical effects, both real [illegible] subjective, who has seen the phenomenon at its [illegible] will have any doubt about its reality. There is no question in my mind but that the usual [illegible] ation [illegible] pheric dispersion) is quite correct. [illegible] main question to answer is: Why is it seen so [illegible] even under conditions which appear to be the favourable?

[illegible] have crossed the ocean some thirty times and have [illegible] ed for the "ray" at every favourable opportunity, [illegible] then I mean clear sky, no haze or clouds on the [illegible] at sunset, and a calm sea, and yet I have [illegible] it on only three or four occasions, and only [illegible] when it was really striking. This occasion was [illegible] eastward trip of the *Homeric* sailing from New [illegible] June [illegible] 1925. The colour of the vanishing [illegible] was a vivid emerald green. [illegible] On other [illegible] I have observed evidence of the [illegible] colour change was from red or [illegible] yellow.

[illegible] that the determining factor is the [illegible] of the air and the ocean. Warm [illegible] would flatten the trajectory of the [illegible] the sun to set abnormally early, [illegible] refraction in cases of desert mirage, [illegible] curvature of the rays is reversed, [illegible] water and warm air, on the contrary, the [illegible] refractive index would be increased, [illegible] the rays augmented, and sunset would [illegible] a greater opportunity for atmo- [illegible] come into play.

[illegible] courtesy of Capt. Parker, of the [illegible] been furnished with data regarding [illegible] temperatures [illegible] On the [illegible] observed the ray the temperatures [illegible] water were practically the same at sunset. [illegible] other three favourable evenings, on which we [illegible] to see any trace of the phenomenon, the ocean [illegible] to fourteen degrees warmer than the [illegible] I hope that this note may prompt [illegible] the green ray to secure data on the [illegible] and water temperature, both for occasions on [illegible] seen, as well as those on which it is [illegible].

R. W. WOOD.

[illegible] University,
[illegible] more.

A New Type of Secondary Radiation.

If we assume that the X-ray scattering of the [illegible] unmodified [illegible] observed by Prof. Compton corre- [illegible] to the normal or average state of the atoms [illegible] molecules, while the "modified" scattering of [illegible] wave-length corresponds to their fluctuations [illegible] that state, it would follow that we should expect [illegible] in the case of ordinary light two types of scatter- [illegible] determined by the normal optical properties [illegible] the atoms or molecules, and another representing [illegible] effect of their fluctuations from their normal [illegible]. It accordingly becomes necessary to test [illegible] whether this is actually the case. The experiments [illegible] have made have confirmed this anticipation, and

shown that in every case in which light is scattered by the molecules in dust-free liquids or gases, the diffuse radiation of the ordinary kind, having the same wave-length as the incident beam, is accompanied by a modified scattered radiation of degraded frequency.

The new type of light scattering discovered by us naturally requires very powerful illumination for its observation. In our experiments, a beam of sunlight was converged successively by a telescope objective of 18 cm. aperture and 230 cm. focal length, and by a second lens of 5 cm. focal length. At the focus of the second lens was placed the scattering material, which is either a liquid carefully purified by repeated distillation *in vacuo* or its dust-free vapour. To detect the presence of a modified scattered radiation, the method of complementary light-filters was used. A blue-violet filter, when coupled with a yellow-green filter and placed in the incident light, completely extinguished the track of the light through the liquid or vapour. The reappearance of the track, when the yellow filter is transferred to a place between it and the observer's eye is proof of the existence of a modified scattered radiation. Spectro[illegible] confirmation is also available.

[illegible] different [illegible] in this way, and [illegible] effect in greater or less degree. That the effect [illegible] scattering and not [illegible] in the first place by its feebleness in comparison with [illegible] primary scattering, and secondly by its polarisation [illegible] in many cases quite strong and comparable with the polarisation of the primary scattering. [illegible] investigation is naturally much more difficult in the case of gases and vapours, owing to the [illegible] feebleness of the effect. Nevertheless, when the vapour is of sufficient density, for example with ether or amylene, the modified scattering [illegible] demonstrable.

C. V. RAMAN.
K. S. KRISHNAN.

210 Bow Bazar Street,
Calcutta, India,
Feb. 16.

Land-locked Salmon.

[illegible] land-locked [illegible] generally [illegible] of salmon [illegible] received in NATURE of Mar. 17 [illegible] lakes Wenern and Ladoga, and even for the [illegible] The word [illegible] but the [illegible] is not always true and that it owes [illegible] this circumstance.

[illegible] that Lake Wenern has a stock of salmon [illegible] that it was [illegible] the falls first became impassable [illegible] prevented [illegible] ascending and they [illegible] so that none would [illegible]. It seems clear that in the days when the lake was accessible from the sea and salmon went through [illegible] some of the smolts that descended into the lake [illegible] sufficiently good substitute for the sea to stay there, and so [illegible] became [illegible] Similarly [illegible] some of the smolts reaching the [illegible] stay and feed on the [illegible] and pelagic crustacea, and [illegible] lake-salmon [illegible] impassable.

The trout forms fresh-water colonies in [illegible] that it enters [illegible] this species the term "land-locked" is never used. On this side of the

Atlantic the [illegible] tion to the [illegible] only in [illegible] lakes with [illegible] with [illegible] to [illegible] no [illegible] readily.

British M[illegible]

Anomalo[illegible]

[illegible]

Nationa[illegible]

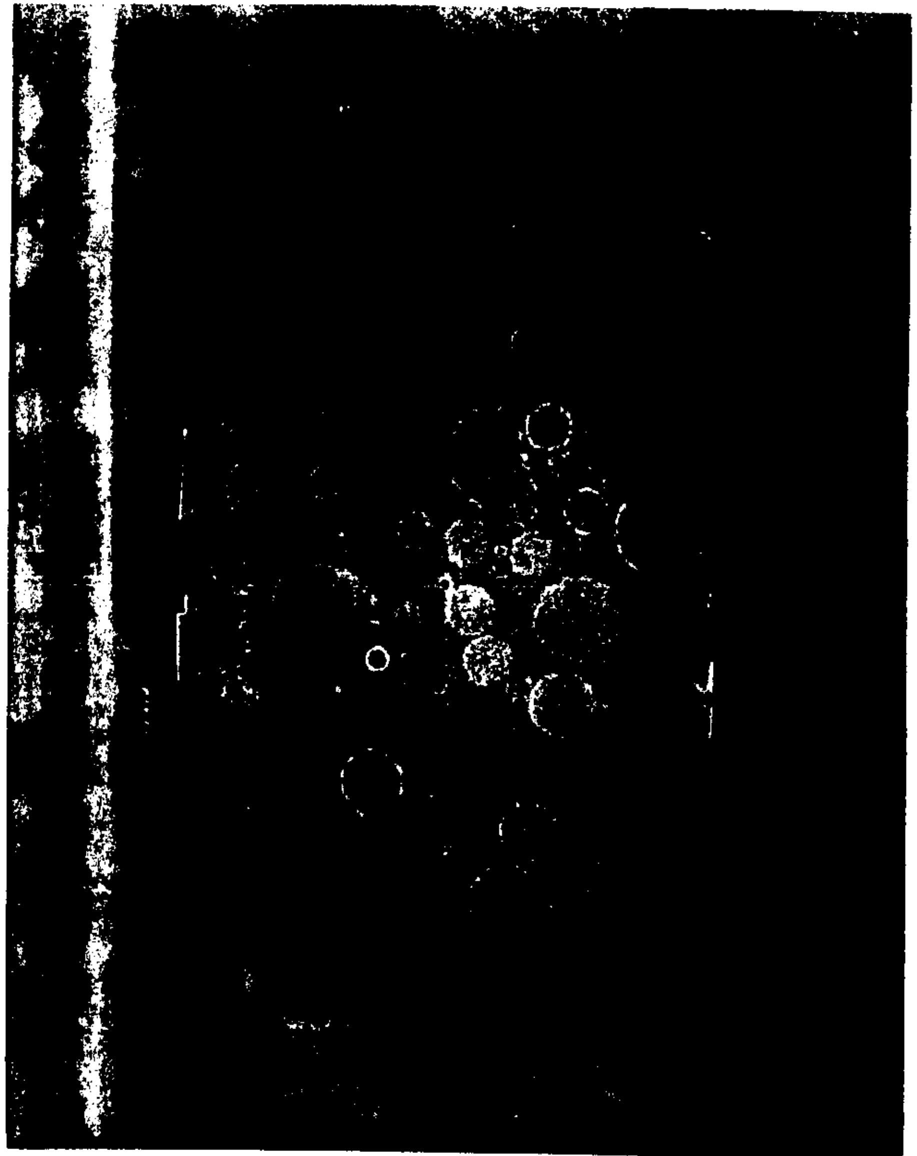

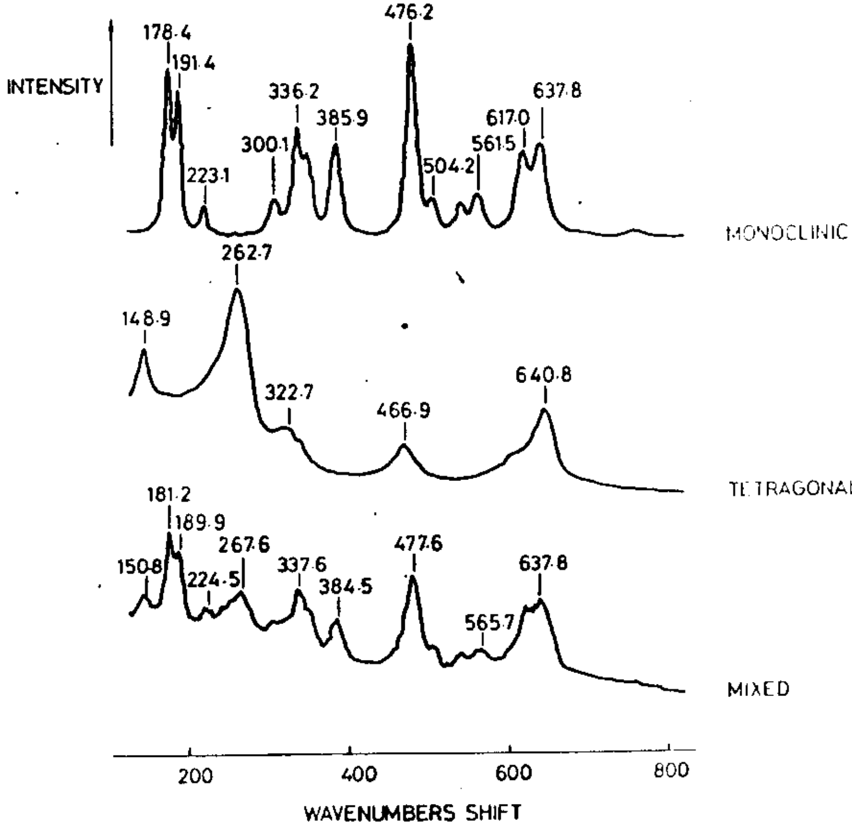

INTENSITY
178·4
191·4
223·1
300·1
336·2
385·9
476·2
504·2
561·5
617·0
637·8
MONOCLINIC
262·7
148·9
322·7
466·9
640·8
TETRAGONAL
181·2
189·9
150·8
224·5
267·6
337·6
384·5
477·6
565·7
637·8
MIXED
200
400
600
800
WAVENUMBERS SHIFT

5

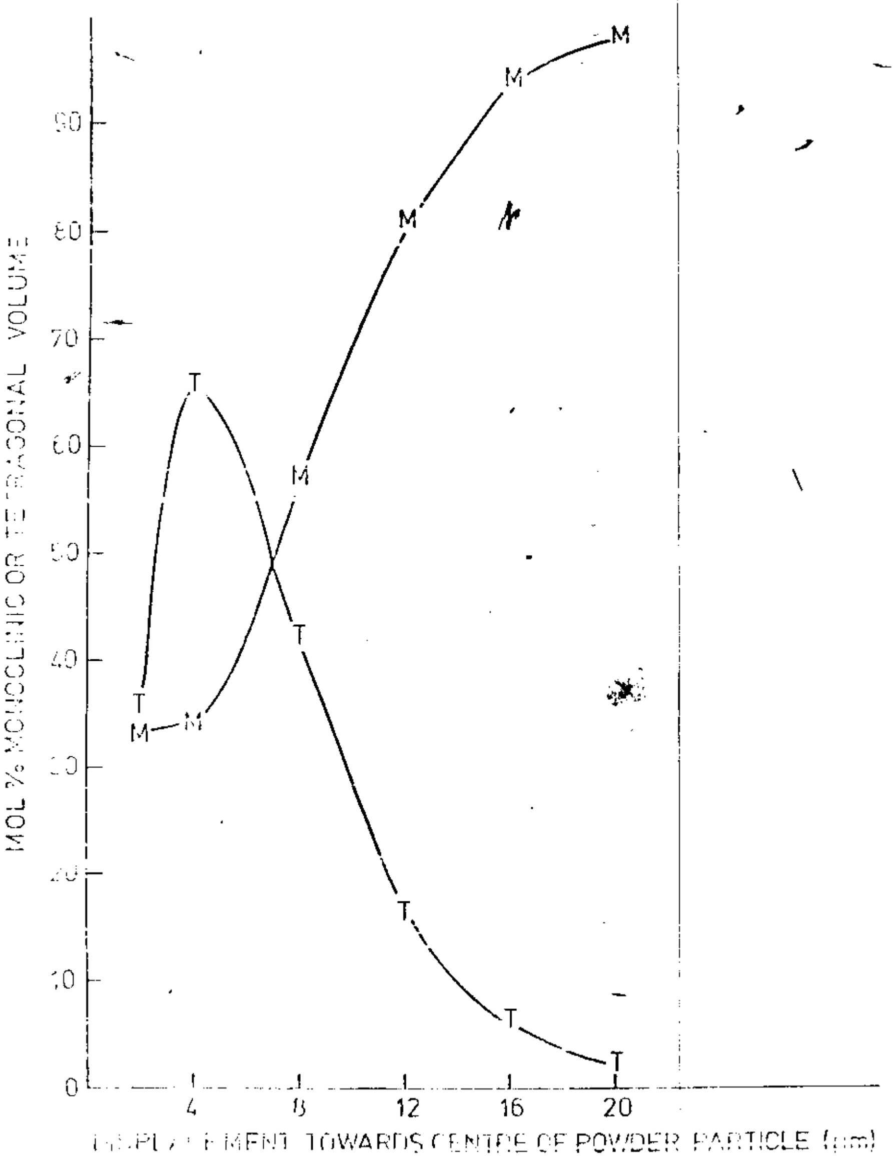

RAMAN ANALYSIS OF 10% wt Y_2O_3 SOL/GEL PRECURSOR PLOT SHOWING RELATIVE PERCENTAGES OF MONOCLINIC AND TETRAGONAL PHASES BASED ON NORMALISED RAMAN INTENSITIES OF THE 251 cm^{-1} (T) AND 381 cm^{-1} (M) BANDS

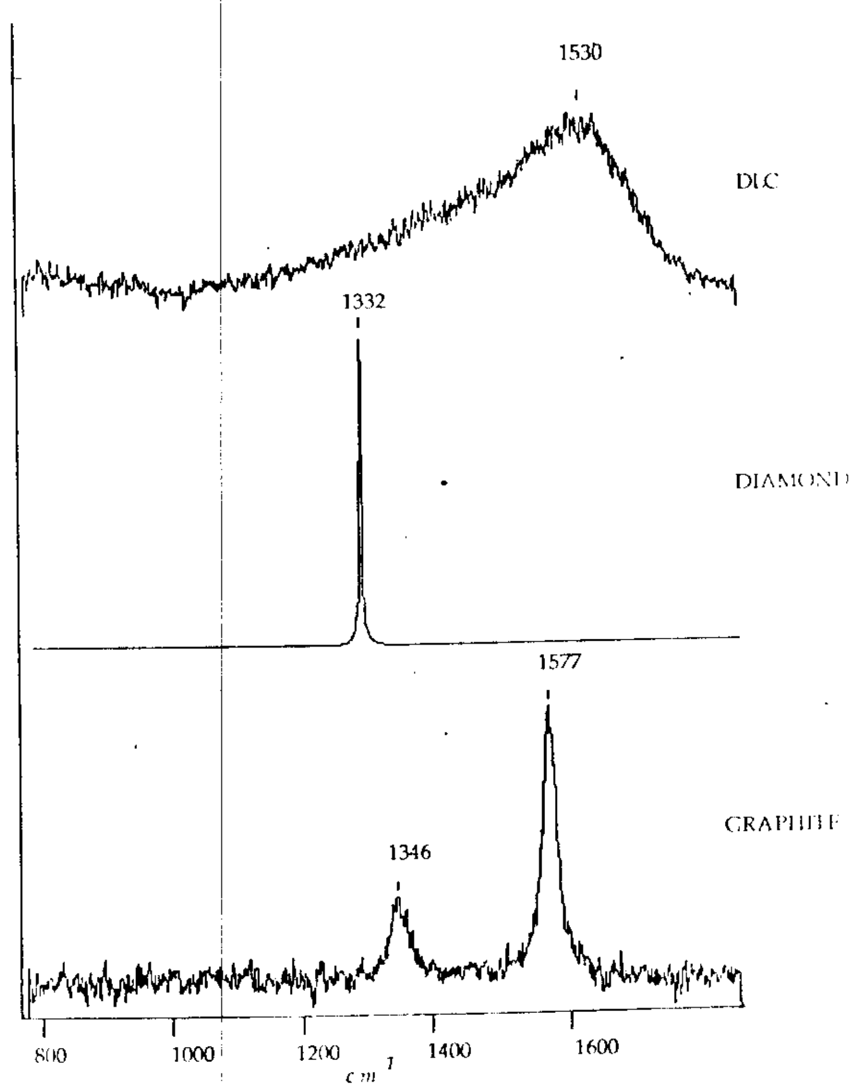

Raman spectra of diamond, graphite and diamond like carbon 'DLC'.

6

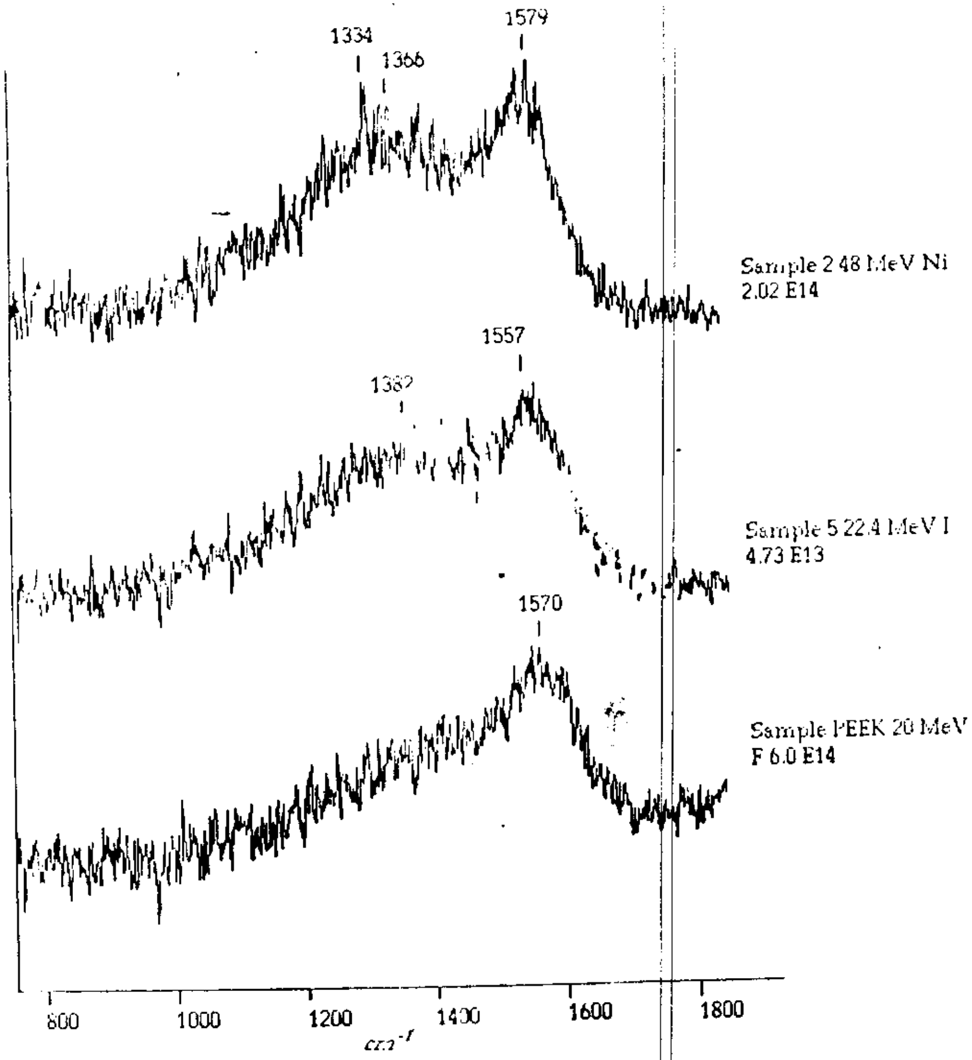

Raman spectra of irradiated polymers as a function of dose and energy, showing sp^2 and sp^3 and diamond sp^3 bonding.

ELECTRON PROBE MICROANALYSIS KEY POINTS

- quantitative elemental analysis for Z > 4 (WD) and Z >11 (ED)
- better than 1 micron spatial and depth resolution
- point, line and image maps possible
- nominally non-destructive
- used in moderate vacuum
- almost all materials are suitable for EPMA

EMPA
Electron Microprobe Analysis

PROCESS

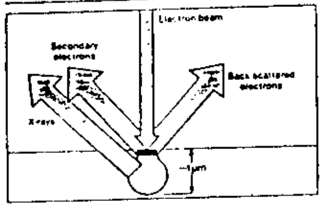

AN EXAMPLE

EMPA is used to investigate elemental composition in solids eg cements. Cements can be used for intermediate radioactive waste encapsulation

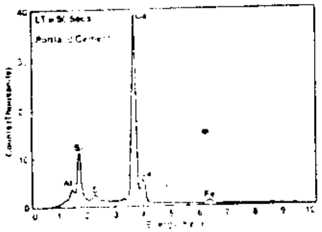

EMPA

A JEOL 8600 scanning microprobe

A Cameca CAMEBAX scanning microprobe

- ☐ Fully quantitative analysis
- ☐ Generation of multi-element line scans
- ☐ Digital mapping of elemental distributions
- ☐ Automated feature detection

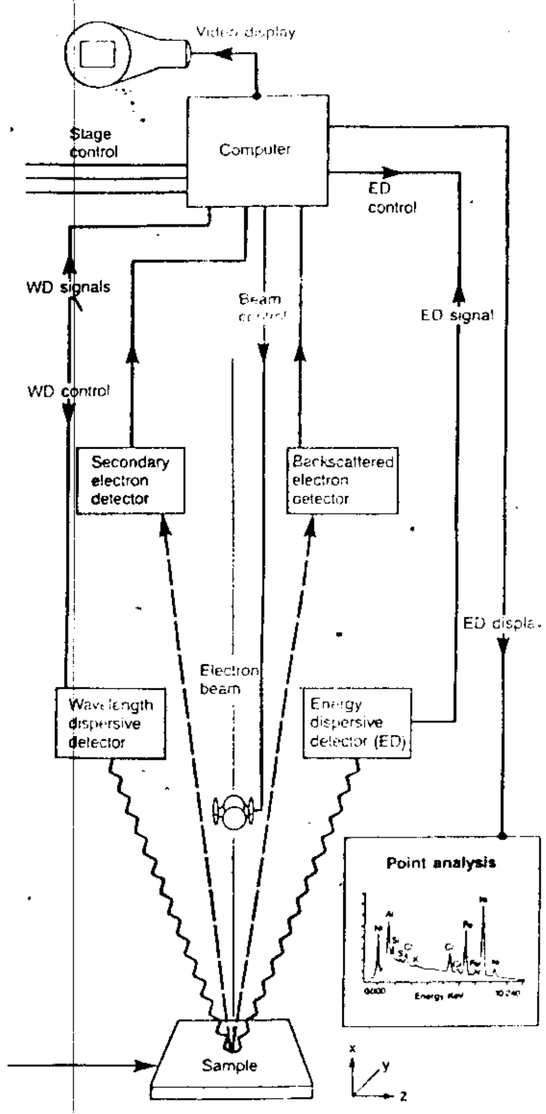

Schematic diagram of a Cameca Camebax electron microprobe

PROPERTIES OF SUPERCONDUCTORS

Zero Resistance

When superconductors are cooled below their critical temperature they have zero electrical resistance

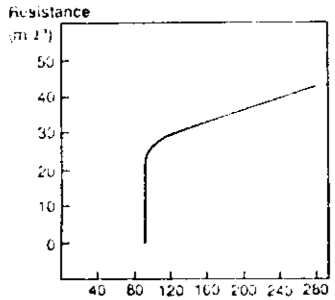

The temperature dependence of the electrical resistance of a sample of $YBa_2Cu_3O_7$ - a zero resistance state is achieved at about 90K.

The Meissner Effect

When the temperature (T) of a superconductor is above its critical temperature (T_c), an external magnetic field will pass through it.

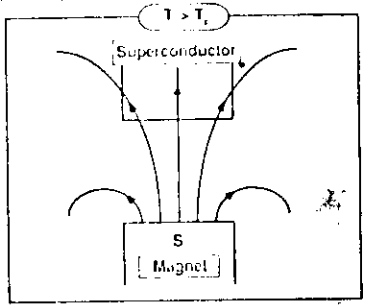

When a superconductor is cooled below its critical temperature it exhibits perfect diamagnetism, it is repelled by a magnetic field.

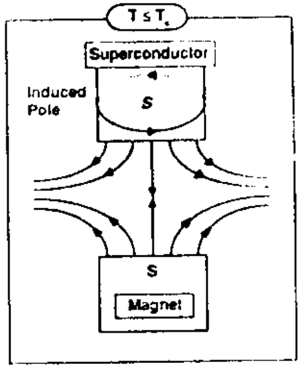

When a superconductor is cooled to its critical temperature, or below, it exhibits perfect diamagnetism - **The Meissner Effect** - an external magnetic field will induce an electric current to circulate within the superconductor. This circulating current generates a magnetic field in such a direction that it opposes the force that is creating it (Lenz's Law). As there is zero electrical resistance within the superconductor the induced magnetic field and the electric current and will remain until the temperature of the superconductor is greater than its critical temperature. The external field and the induced magnetic field are in opposite directions and so repel each other, hence the levitation.

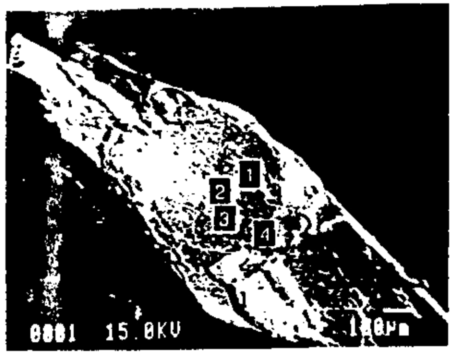

Sample 1

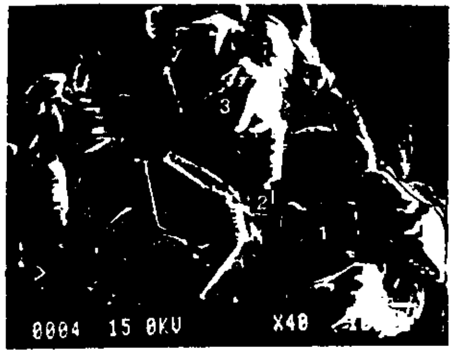

Sample 3

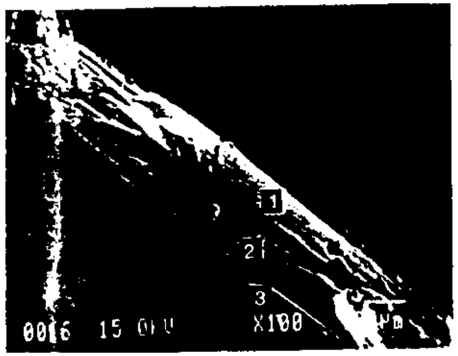

Sample 4

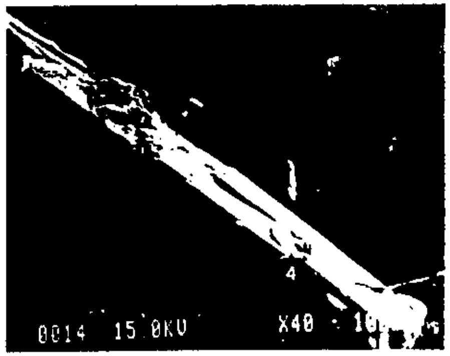

Sample 4

Sample 6

Secondary electron images of samples showing positions of EMPA measurements.

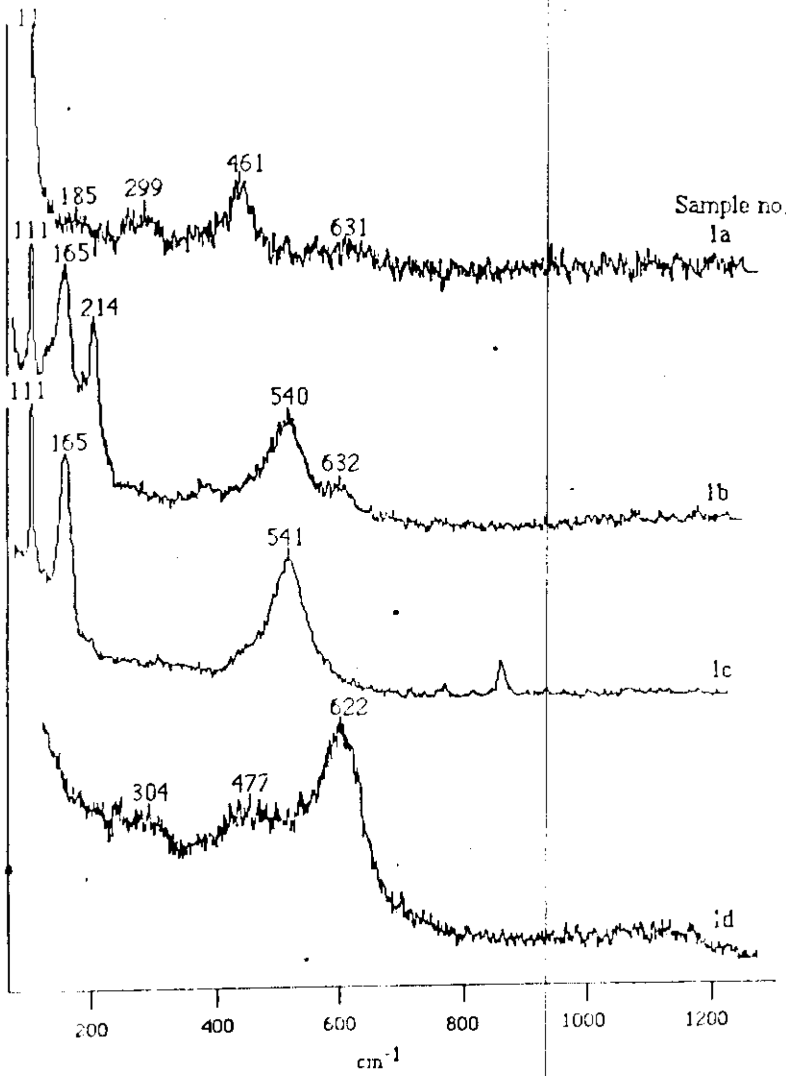

A single sample obtained from a CuO flux was analysed in four different positions. The Raman spectra from each position are significantly different.

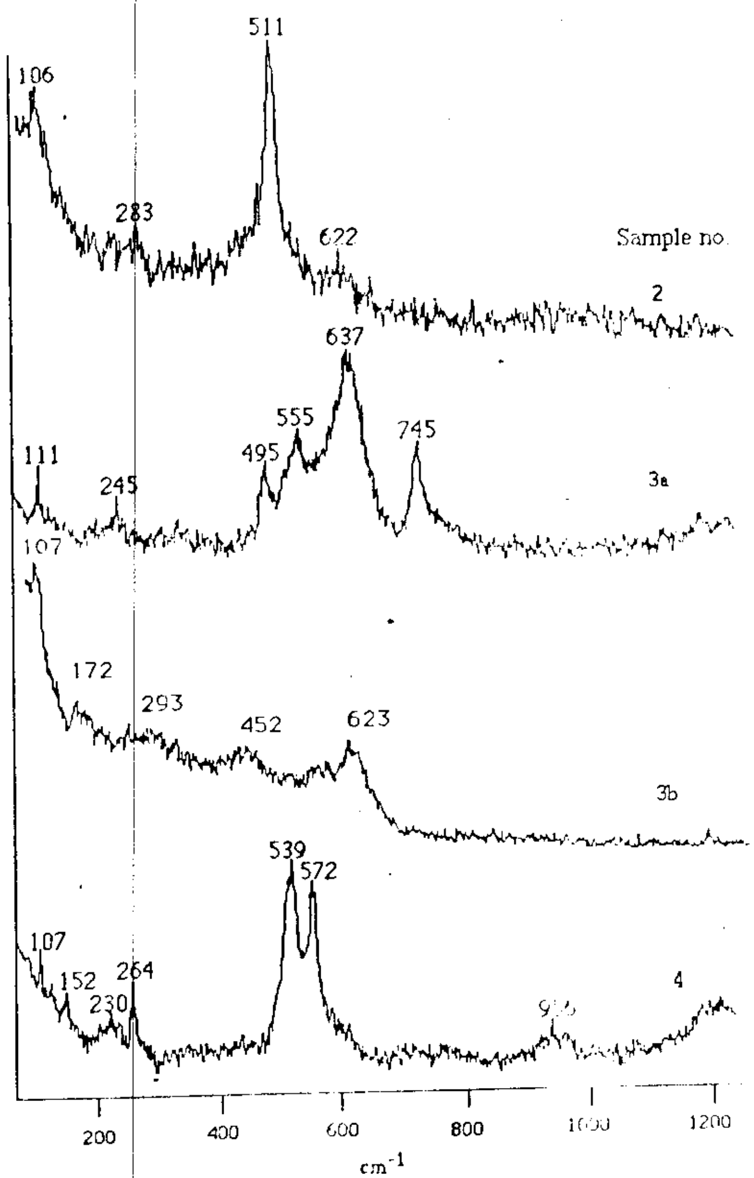

Raman spectra of crystals 2,3 and 4, obtained from CuO flux. Samples 3 and 4 were from the same batch, sample 2 from another.

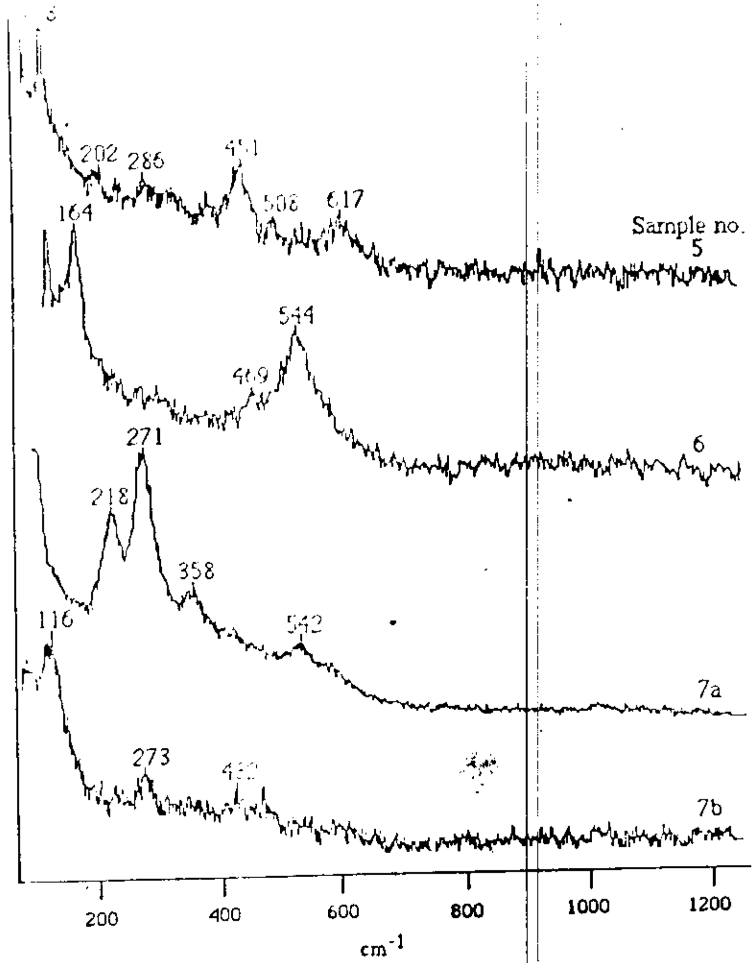

Raman spectra of three crystals obtained by growth from a KCl flux. Samples 6 and 7 were from the same batch whereas sample 5 was from a separate batch. Spectrum (b) from sample 7 was recorded with a defocussed spot, averaging a larger area.

Table 1

Summary of results with chemical phases

Sample no. / Point	EMPA Atom % Bi/Sr/Ca/Cu/O	Total w/%	Phase	RAMAN Sample no. / Point	RAMAN Frequency (cm^{-1})
1/1	32 : 12 : 3 : 12 : 41	93		1/a	113, 299, 461, 631
1/2	32 : 10 : 2 : 12 : 44	91		1/b	111, 165, 541
1/3	14 : 14 : 5 : 14 : 52	95	$Bi_2Sr_2CaCu_2O_8$	1/c	111, 165, 541
1/4	30 : 12 : 3 : 9 : 47	90		1/d	304, 477, 622
3/2	14 : 10 : 5 : 13 : 57	93	$Bi_2Sr_2CaCu_2O_8$	3/b	107, 172, 293, 452, 623
3/3	14 : 14 : 5 : 14 : 52	95	$Bi_2Sr_2CaCu_2O_8$		
3/4	18 : 17 : 7 : 18 : 40	93			
4/3	0 : 13 : 14 : 30 : 43	90	$SrCaCu_3O_4$	4/a	107, 152, 230, 264, [illegible], 572, 956
4/4	0 : 16 : 15 : 33 : 37	92			
5				5/a	108, 451, 617
6/2	20 : 11 : 12 : 16 : 41	90		6/a	164, 544
7				7/a	218, 271, 358, 542
7				7/a	116, 273 (defocussed)

-Group theory of $Bi_2Sr_2CaCu_2O_8$

- Factor group- D_{2h}
- Symmetry- Distorted tetragonal
- Raman active vibrational modes-

$$6A_{1g} + B_{1g} + 7E_g$$

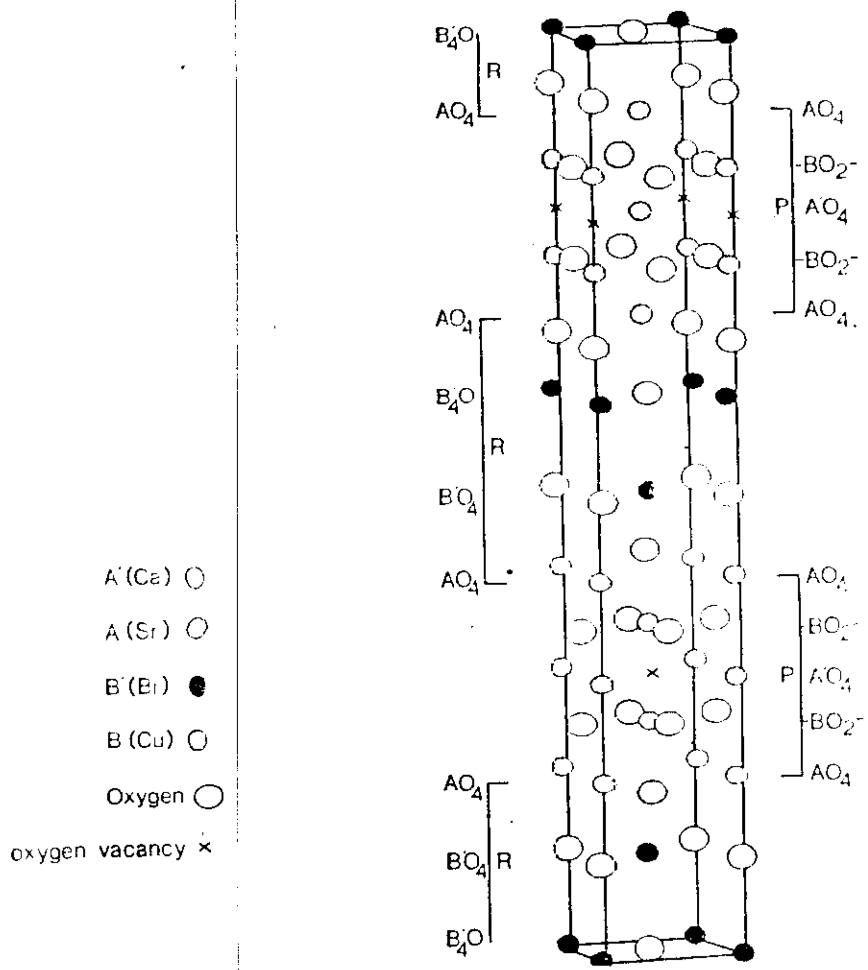

Structural unit cell of $Bi_2Sr_2CaCu_2O_8$ showing perovskite octahedra (P) and rock salt octahedra (R)

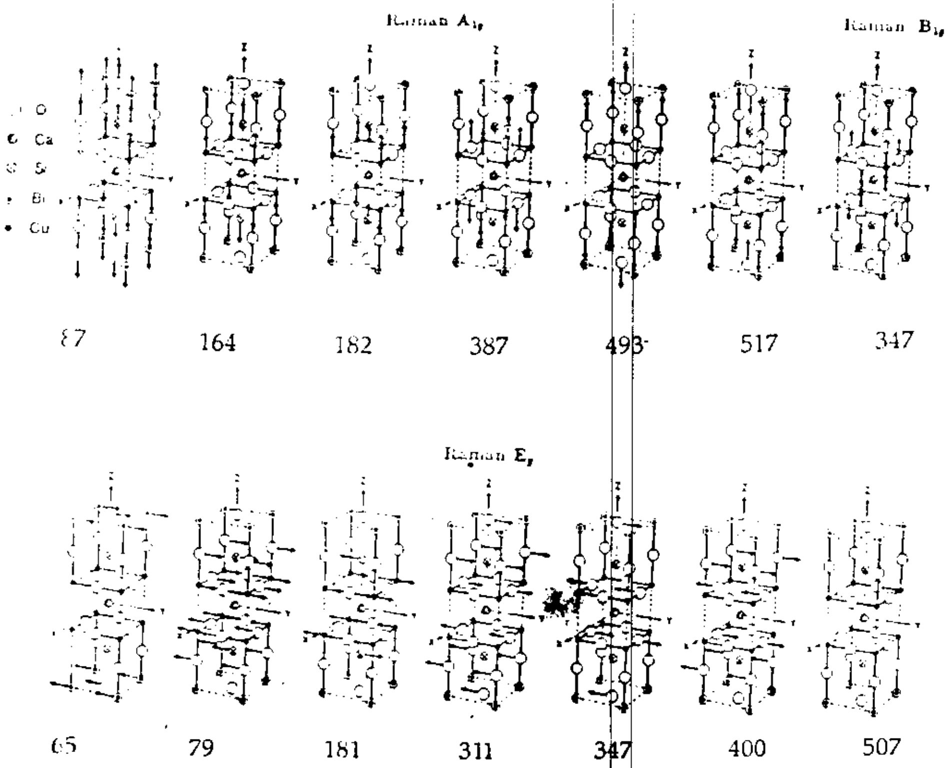

PHYSICAL REVIEW B VOLUME 39, NUMBER 4 1 FEBRUARY 1989

Calculation of Raman- and infrared-active modes of $Bi_2CaSr_2Cu_2O_8$

J. Prade,* A. D. Kulkarni, and F. W. de Wette
Department of Physics, University of Texas, Austin, Texas 78712

U. Schröder
Universität Regensburg, D-8400 Regensburg, Federal Republic of Germany

W. Kress
Max-Planck-Institut für Festkörperforschung, D-7000 Stuttgart 80, Federal Republic of Germany

(Received 6 September 1988)

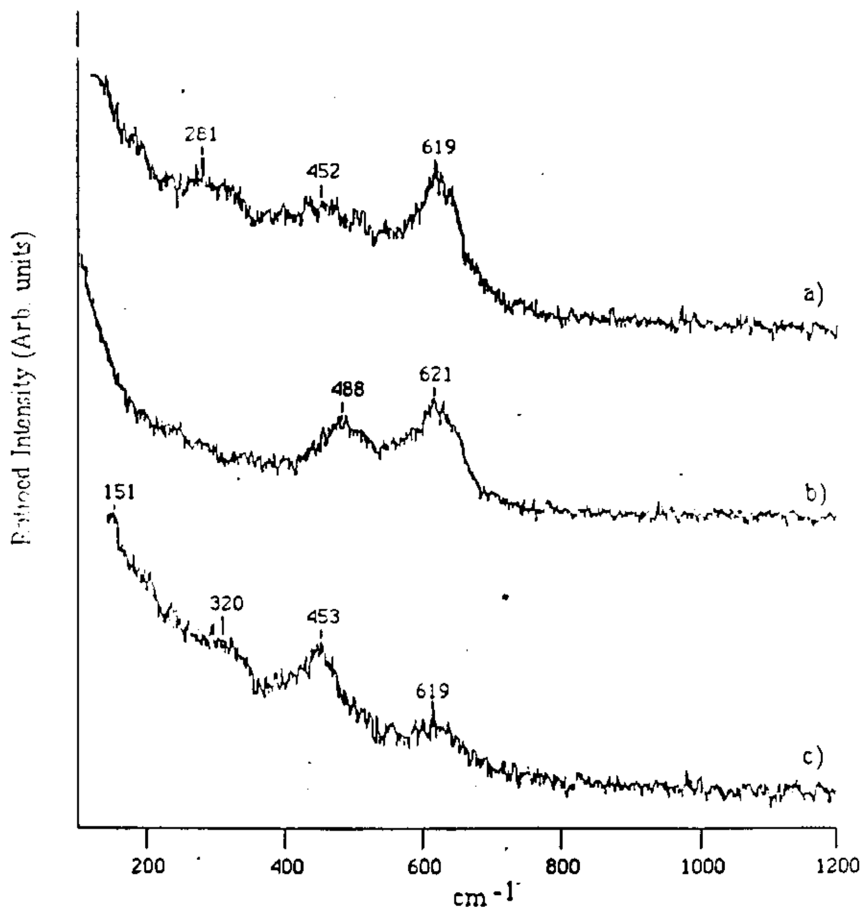

Raman excitations observed after exposure to laboratory atmosphere of single crystal face. Curves (a), (b), (c) were obtained from different, but randomly chosen, locations.

Micrograph of freshly cleaved crystallite face, analysed by Raman microscopy (length bar=80 µm).

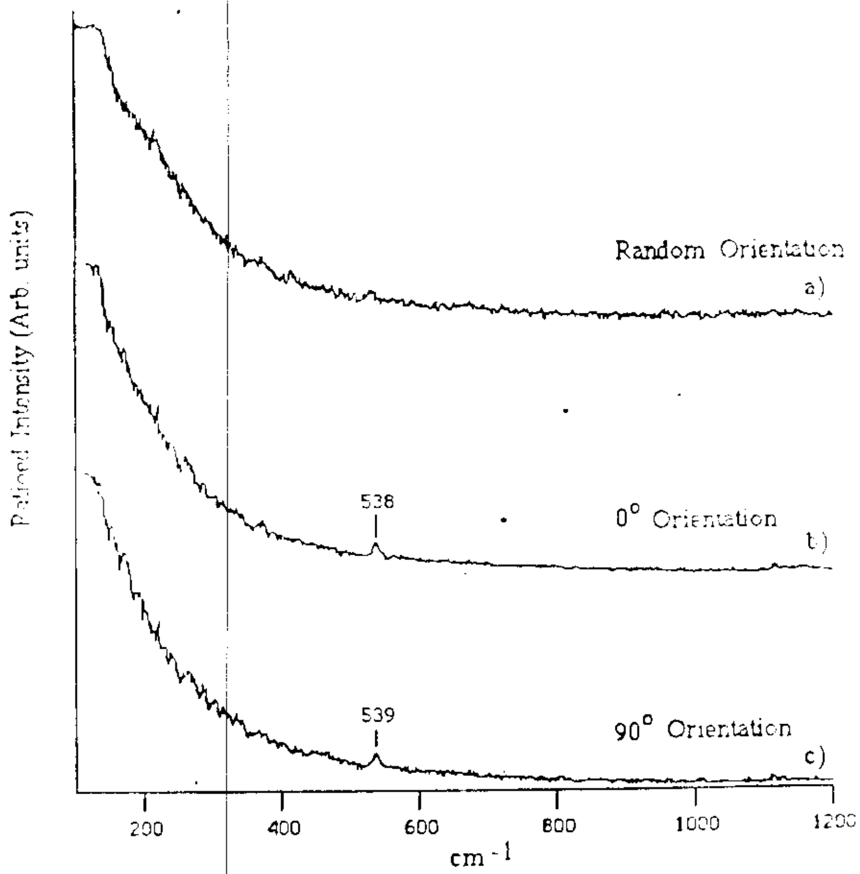

Raman spectra for a freshly cleaved single crystal at (a) random ab plane orientation, and (b) and (c) 90° rotation in the ab plane with respect to a crystal edge (see Figure 2).

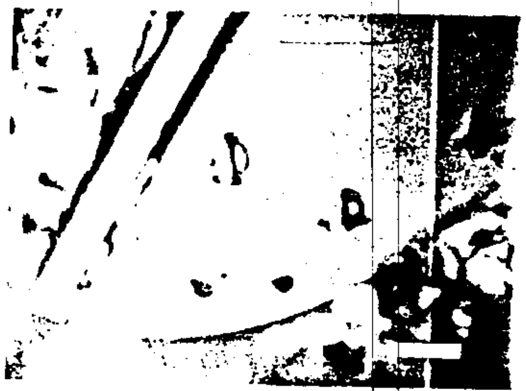

Micrograph of crystallite face after 0.5 hr saturated steam attack.

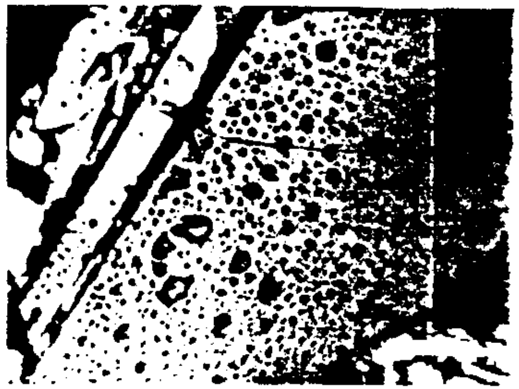

Micrograph of crystallite face after 10 hrs of saturated steam attack.

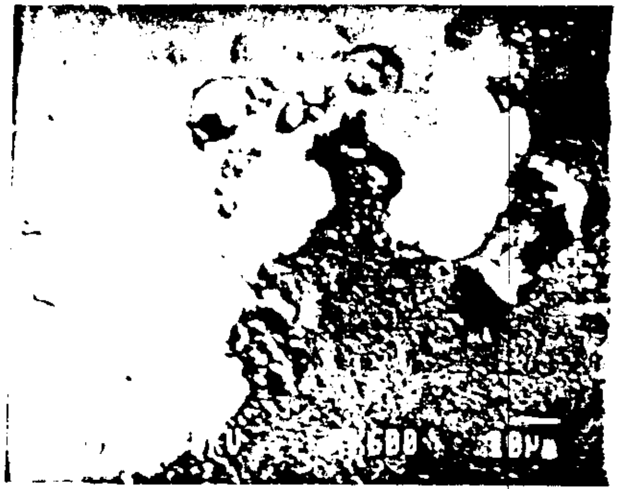

SEM image of crystallite face after 10hrs of saturated steam attack.

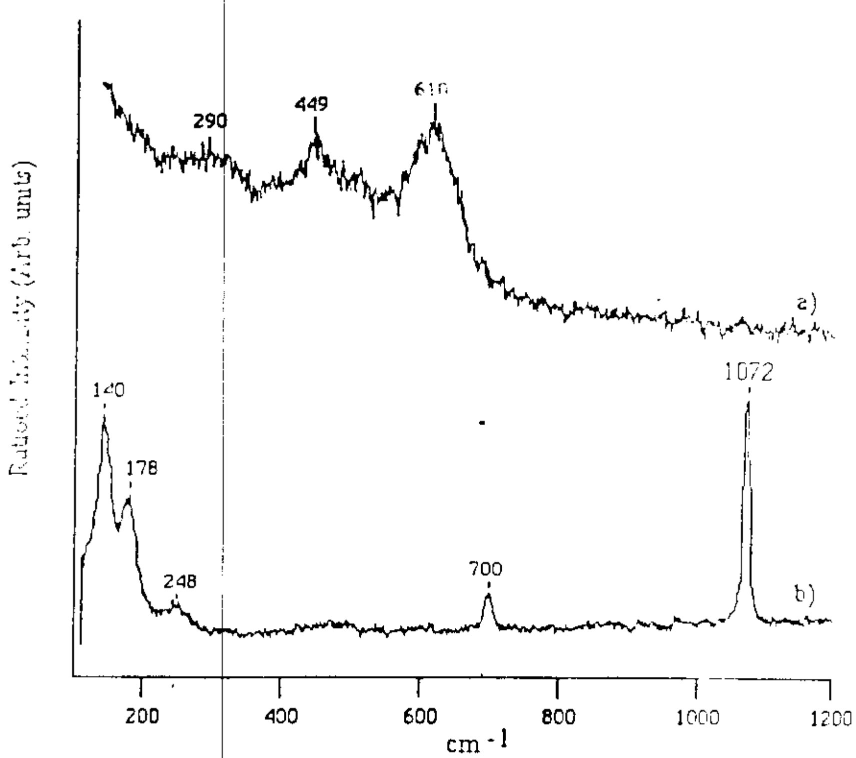

Raman features observed during the early (a) and late (b) stages of degradation by saturated steam.

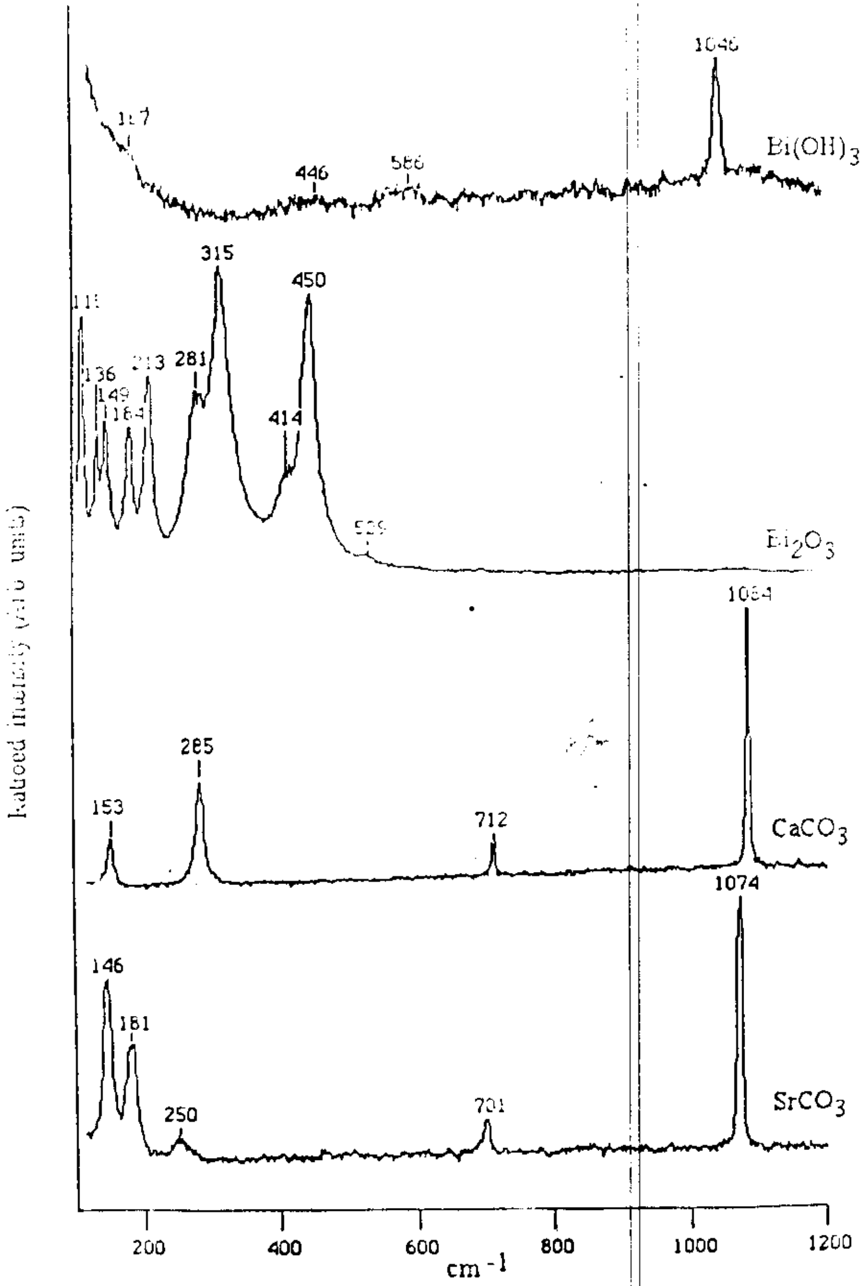

The results of Raman analysis of model degradation compounds. The sharp feature at 1046 cm^{-1} in the spectrum of Bi(OH)$_3$ is due to nitrate contamination.

THEORY OF RAMAN SCATTERING

$$\underline{P} = \underline{\alpha} \cdot \underline{e}$$

$\underline{P}$	induced dipole vector
$\underline{\alpha}$	polarisability tensor
$\underline{e}$	laser electric vector

Generally,,

$$\begin{matrix} x \\ y \\ z \end{matrix} \qquad \begin{matrix} a & b & c \\ d & e & f \\ g & h & i \end{matrix} \qquad \begin{matrix} x \\ y \\ z \end{matrix}$$

-For phonon scattering, α is always symmetric

-Every vibrational mode has a particular scattering tensor, whose symmetry reflects that of the mode

EXPERIMENTAL DETAILS

- Align crystal with respect to laboratory axes and laser beam electric vector with respect to the Raman microscope

- PORTO notation defines the experiment:

A (B C) D

A- direction of incident laser beam
D- direction of collection of scattered light
B- polarisation of laser electric vector
C- polarisation of scattered light analyser

- We can now select the elements of the polarisability tensor detected and hopefully identify the Raman vibrations as specific modes.

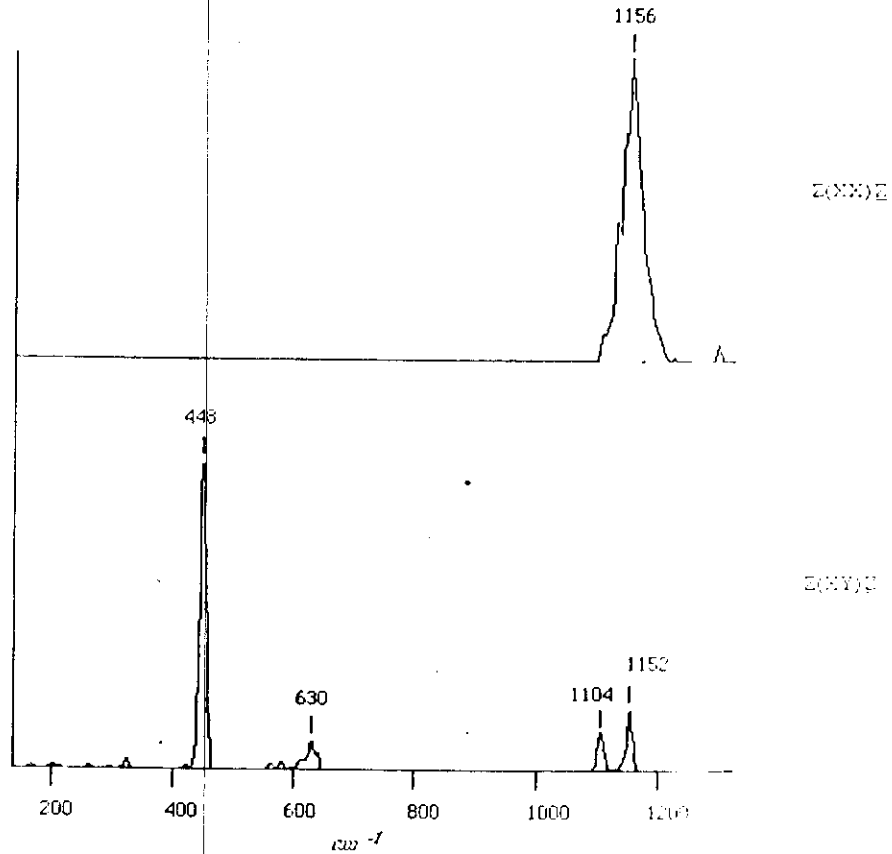

Polarised Raman spectra of single crystal uranium dioxide. Porto notations show the experimental conditions.

URANIUM DIOXIDE

STRUCTURE: Fluorite

SPACE GROUP: O_h^5

Group theory : $T_{2g} + T_{1u}$ vibrational modes

Scattering tensor α :

$$T_{2g} = \begin{matrix} 0\,0\,0 \\ 0\,0\,d \\ 0\,d\,0 \end{matrix} \qquad \begin{matrix} 0\,0\,d \\ 0\,0\,0 \\ d\,0\,0 \end{matrix} \qquad \begin{matrix} 0\,d\,0 \\ d\,0\,0 \\ 0\,0\,0 \end{matrix}$$

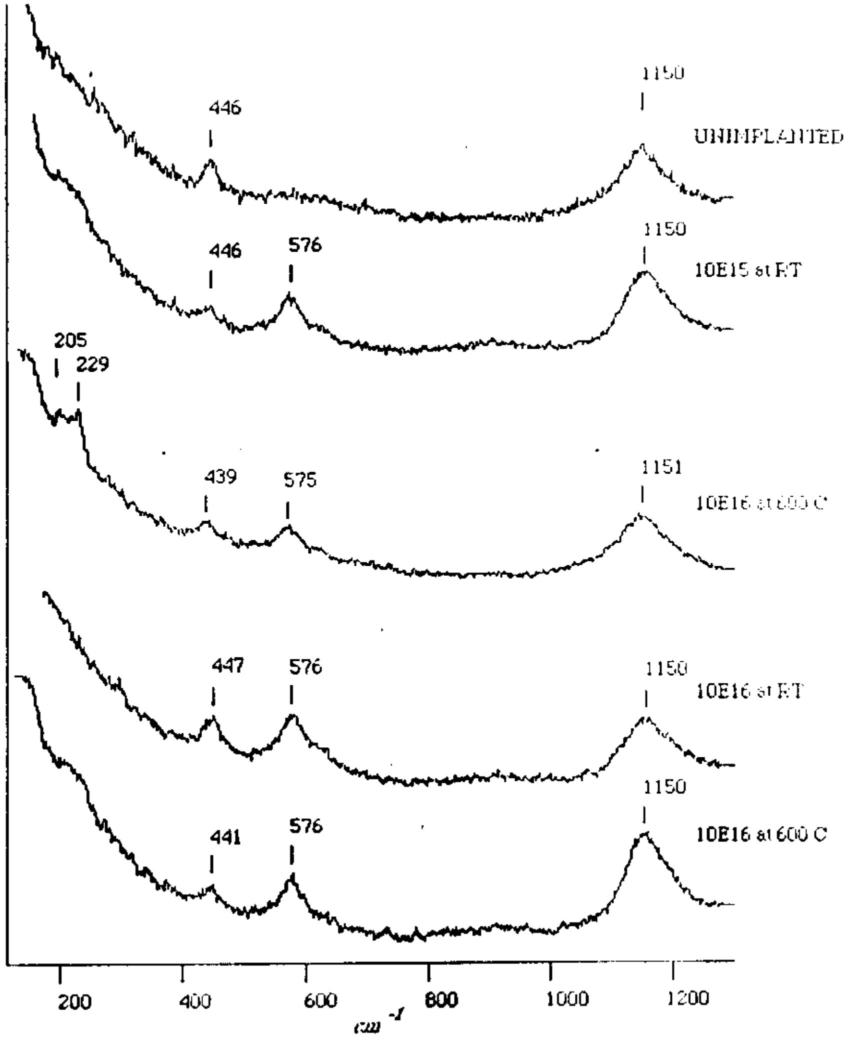

Raman spectra of Kr ion implanted uranium dioxide pellets. Implantation was carried out at the indicated doses (cm^{-2}), at 200 KeV energy and at the temperatures given. The calculated range of the implant is 400 Å.

19

3. RESULTS

Figure 4 shows the measured dispersion curves for the symmetric directions [00ζ], [ζζ0], and [ζζζ], or, in group-theory notation (see Appendix 1), Δ, Σ, and Λ. The frequencies of some selected normal modes are given in Table I. The experimental uncertainty is generally ~2 or 3% in frequency, but may be considerably larger for the branches of highest frequency.

TABLE I

Frequencies of selected normal modes of vibration in uranium dioxide at 296 °K (No space-group symbol is shown for the Γ_{15} modes at $q = 0$ which are split by the macroscopic electric field)

Wave-vector coordinates ($\zeta_1, \zeta_2, \zeta_3$)	Mode	Frequency (units 10^{12} c.p.s.)
(0, 0, 0)	(Longitudinal)	16.7 ±0.60
	Γ_{25}'	13.42±0.16
	(Transverse)	8.52±0.11
(0, 0, 1.0)	M_1	18.2 ±1.0
	M_4'	13.68±0.21
	M_4	6.98±0.12
	M_2, M_5'	5.27±0.08
	M_5	3.27±0.08
(0.5, 0, 0)	$\Sigma_1(01)$	16.8 ±0.7
	$\Sigma_1(02)$	14.0 ±0.5
	$\Sigma_3(01)$	9.83±0.29
	$\Sigma_1(02)$	6.49±0.11
	$\Sigma_3(4)$	4.64±0.07
	$\Sigma_3(4)$	4.23±0.06
(0.5, 0.5, 0.5)	L_2'	17.2 ±1.2
	L_1	12.6 ±0.4
	L_3'	12.2 ±0.4
	L_3	10.57±0.25
	L_3'	5.21±0.10
	L_3'	2.75±0.04

446 cm^{-1}
RAMAN T_{2g} mode

It is interesting to note that the longitudinal acoustic ($\Delta_1(A)$) and the longitudinal optic (Δ_2') branches are accidentally degenerate at the zone boundary (M) within the limits of experimental error, a fact which impeded precise frequency measurements in this region.

The steeply rising Δ_2' branch shows that there is no gap in the frequency distribution between the optic and the acoustic modes such as one might expect as a result of the large difference in mass between oxygen and uranium. Detailed calculations of the distribution (Fig. 5, Section 4) show that there is probably no gap in any part of the frequency spectrum.

The initial slopes of the acoustic branches are consistent with independent measurements of the elastic constants (Wachtman *et al.* 1965), and the frequencies of the TO and LO modes at $q = 0$ are consistent with the measured static (Briggs 1964) and high-frequency (Ackermann *et al.* 1959) dielectric constants (ϵ_0 and ϵ_∞ respectively) through the relation (Lyddane *et al.* 1941)

$$\left(\frac{\nu_{LO}}{\nu_{TO}}\right)^2_{q=0} = \frac{\epsilon_0}{\epsilon_\infty}. \tag{3}$$

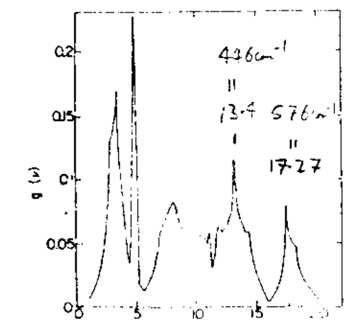

FIG. 5. The frequency distribution function calculated from the best-fit shell model (Model III). The statistical fluctuations in the curve (which is, in fact, a histogram) are too small to be shown in this figure.

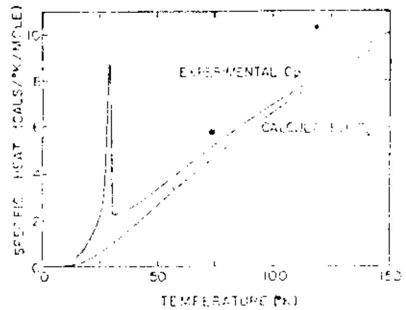

FIG. 6. The measured total specific heat C_p and the calculated lattice specific heat C_v of UO_2. The observed anomaly at 30 °K is due to antiferromagnetic ordering.

measurements. A surprising feature, as shown by Fig. 6, is the magnitude of the magnetic specific heat *above* the antiferromagnetic ordering temperature, T_N. This suggests that there is considerable short-range magnetic order well above T_N. The contribution of the normal modes to the entropy at 298.16 °K is calculated to be 16.12 cal/°K mole, whereas that measured by Jones *et al.* (1952) is 18.63 cal/°K mole. The discrepancy between the calculated specific heat, C_v, and the measured C_p at 250 °K is 0.60 cal/°K mole. This discrepancy probably arises from the difference between C_p and C_v, the anharmonic contribution to the specific heat, and the errors in the measurements of the

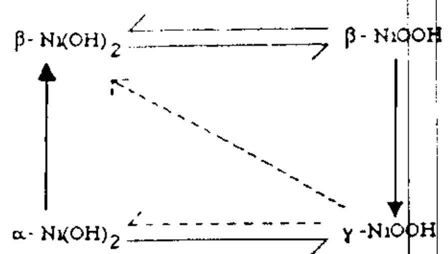

FIG. 1. Nickel oxyhydroxide electrode reaction scheme.

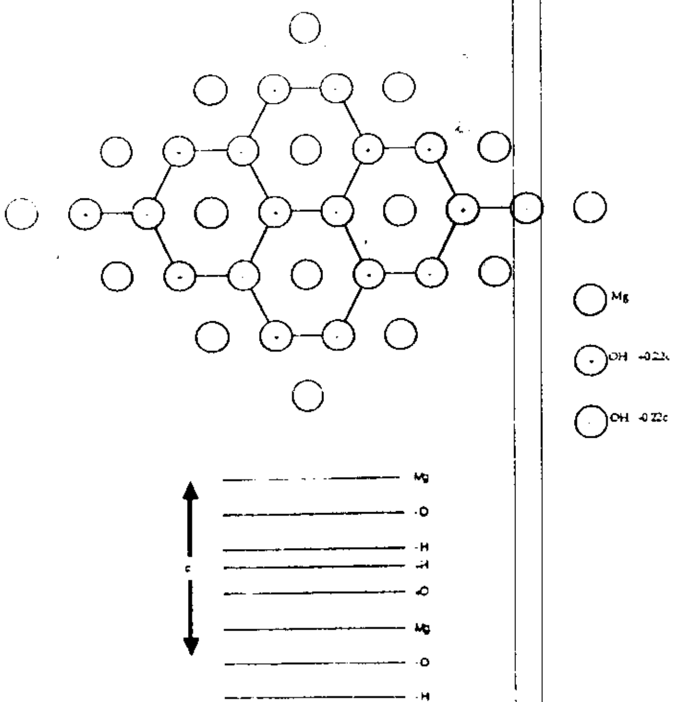

FIG. 2. Graphical representations of the common Brucite structure $Mg(OH)_2$ showing the hexagonal arrangement of the hydroxyl ions around the metal ion and the layered geometry.

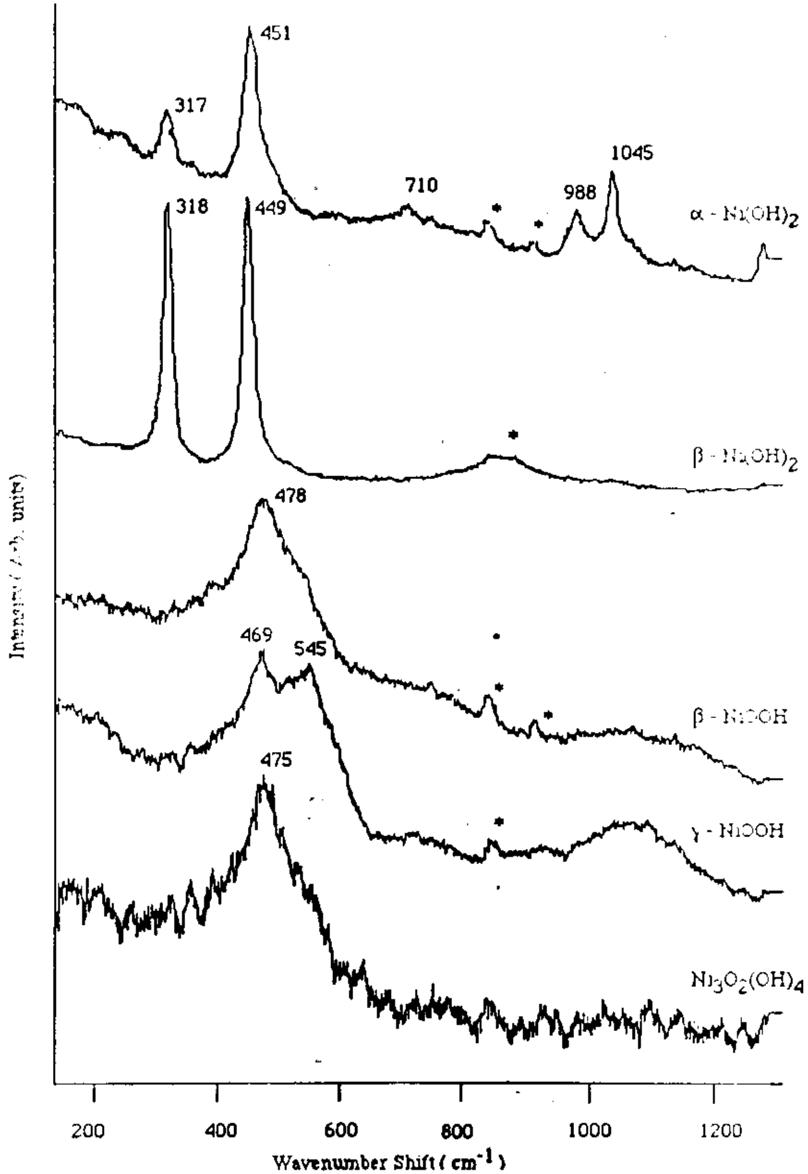

Raman spectra obtained from the reference compounds α - $Ni(OH)_2$, β - $Ni(OH)_2$, β - NiOOH, γ - NiOOH and $Ni_3O_2(OH)_4$ * LRM objective bands.

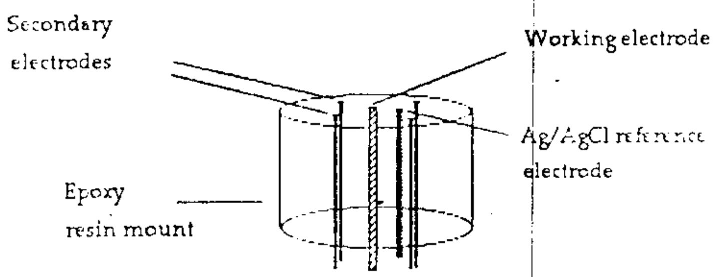

Electrochemical cell for insitu Raman measurements

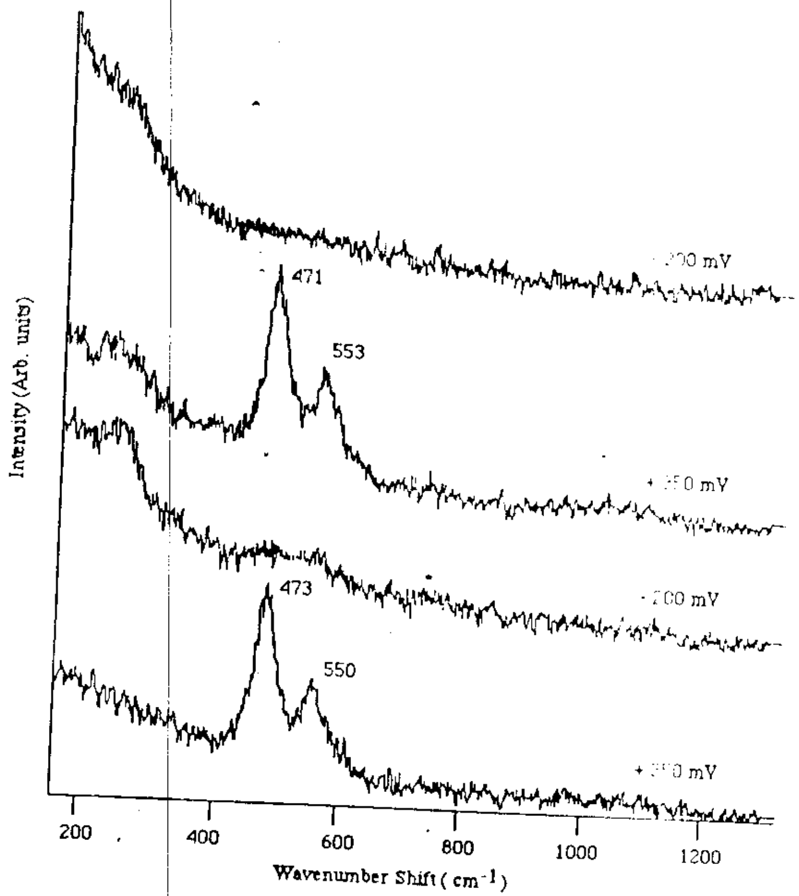

Raman spectra obtained from the surface of a cycled Nickel oxyhydroxide electrode (NOE) with an electrolyte of 8 M KOH $_{(aq)}$.

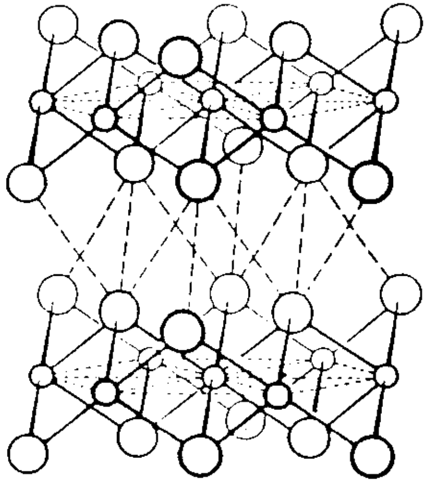

FIG. 9. Portions of two layers of the CdI_2 structure. The small circles represent the metal atoms.

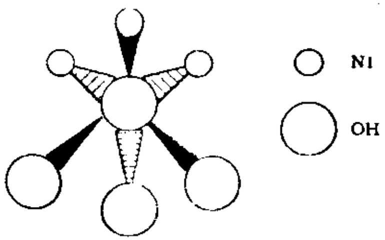

FIG. 10. Unit cell derived from the CdI_2 structure.

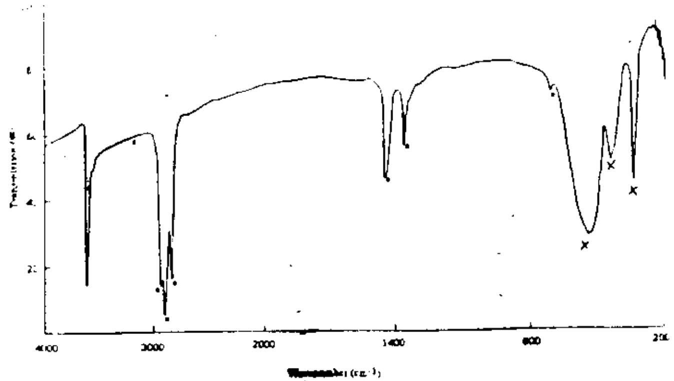

FIG. 5. Infrared spectrum of β-$Ni(OH)_2$. (0) Bands due to nujol.

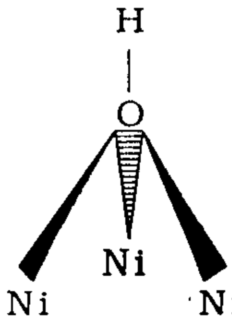

FIG. 11. The spectroscopic unit cell.

C_{3v}	E	$2C_3$	$3\sigma_v$		
A_1	1	1	1	z	$x^2 + y^2, z^2$
A_2	1	1	−1	R_z	
E	2	−1	0	$(x, y)(R_x, R_y)$	$(x^2 - y^2, xy)(xz, yz)$

This gives the reducible representations, χ^R:

C_{3v}	E	$2C_3$	$3\sigma_v$
χ^R_{All}	15	0	3
χ^R_{Trans}	3	0	1
χ^R_{Rot}	3	0	−1

This reduces to give the irreducible representations, Γ:

$$\Gamma_{All} = 4A_1 + A_2 + 5E$$
$$\Gamma_{Rot} = A_2 + E$$
$$\Gamma_{Trans} = A_1 + E.$$

Now,

$$\Gamma_{All} = \Gamma_{Vib} + \Gamma_{Rot} + \Gamma_{Trans}$$
$$\rightarrow \Gamma_{Vib} = 3A_1 + 3E.$$

TABLE IV. Mode assignments for Raman and infrared bands of β-$Ni(OH)_2$.

Frequency (cm^{-1})	Activity	Symmetry type	Assignment
3630	IR	A_1	Asymmetric ν_{OH}
3580	IR, Raman	A_1	Symmetric ν_{OH}
553	IR	E	Deformation δ_{OH}
450	IR, Raman	A_1	ν_{NiO}
350	IR	E	OH libration
318	Raman	E	Ni-OH lattice